ACS APPLIED MATERIALS & INTERFACES

www.acsami.org

Research Article

Biocompatible Parylene-C Laser-Induced Graphene Electrodes for Microsupercapacitor Applications

Ricardo Correia,* Jonas Deuermeier, Maria Rosário Correia, Joana Vaz Pinto, João Coelho,* Elvira Fortunato, and Rodrigo Martins*

Cite This: *ACS Appl. Mater. Interfaces* 2022, 14, 46427−46438

Read Online

ACCESS | Metrics & More | Article Recommendations | Supporting Information

ABSTRACT: Laser irradiation of polymeric materials has drawn great attention as a fast, simple, and cost-effective method for the formation of porous graphene films that can be subsequently fabricated into low-cost and flexible electronic and energy-storage devices. In this work, we report a systematic study of the formation of laser-induced graphene (LIG) with sheet resistances as low as 9.4 Ω/sq on parylene-C ultrathin membranes under a CO_2 infrared laser. Raman analysis proved the formation of the multilayered graphenic material, with I_D/I_G and I_{2D}/I_G peak ratios of 0.42 and 0.65, respectively. As a proof of concept, parylene-C LIG was used as the electrode material for the fabrication of ultrathin, solid-state microsupercapacitors (MSCs) via a one-step, scalable, and cost-effective approach, aiming at future flexible and wearable applications. The produced LIG-MSC on parylene-C exhibited good electrochemical behavior, with a specific capacitance of 1.66 mF/cm^2 and an excellent cycling stability of 96% after 10 000 cycles (0.5 mA/cm^2). This work allows one to further extend the knowledge in LIG processes, widening the group of precursor materials as well as promoting future applications. Furthermore, it reinforces the potential of parylene-C as a key material for next-generation biocompatible and flexible electronic devices.

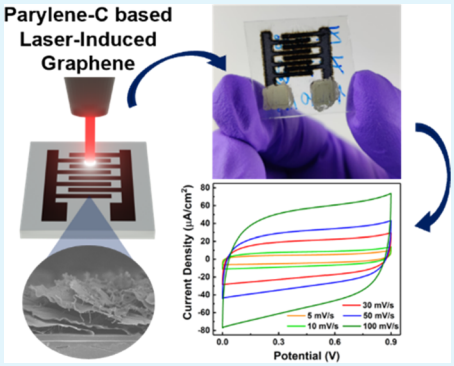

KEYWORDS: *laser-induced graphene, parylene-C, microsupercapacitors, scalable production methods, flexible electronic devices, biocompatible devices*

1. INTRODUCTION

Nowadays, there is a huge demand for portable devices that can wirelessly communicate and sense both physical and chemical parameters in our daily activities, while adhering to sustainable production methods with minimum environmental impact. In this respect, flexible electronics have emerged as a promising technology enabling the fabrication of cost-efficient sensing devices with high flexibility/bendability, conformity, and ultralight weight, leading to new applications in healthcare, wearables, and the Internet of Things (IoT).[1] Nevertheless, to power these circuits, energy needs to be supplied either by wireless transmission methodologies or by embedded energy-harvesting and storage devices.[2] Consequently, the miniaturization and integration of flexible energy-storage devices are crucial for next-generation wearable, compact, and portable flexible electronics.[3] In this regard, lithium-ion batteries (LIBs) have several shortcomings, as their energy per volume tends to rapidly decrease on the micrometer scale. In addition, they also rely on hazardous chemicals as electrolytes, which is not a suitable option for wearable technology.[4] On the other hand, microsupercapacitors (MSCs) hold great promise for future electronic systems as they can operate as standalone devices or be integrated on-chip while retaining their performance.[5] Moreover, MSCs are remarkably safe, present superior power density, stability, and cyclability, have fast charge/discharge capability, and can withstand large mechanical deformations.[3] In addition, the planar two-electrode interdigitated architecture allows the fabrication of small, thin, flexible, lightweight, and easy-to-package devices in contrast to the conventional sandwich configuration.

Among the several candidates for electrode materials for the improvement of MSCs, graphene-based materials have attracted tremendous attention due to their outstanding electrical, mechanical, and morphological properties.[6−8] However, their commercialization has been restrained due to the relatively high cost or complex synthesis and implementation procedures.[9,10] In this scope, the initial work on laser irradiation of polymeric substrates to produce porous graphene films, presented by Tour and co-workers, triggered the development of different new systems based on laser-induced graphene (LIG), including MSCs.[10−12] The high localized temperature and pressure of the laser beam induce the transformation of the precursor material to LIG through a

Received: May 30, 2022
Accepted: July 27, 2022
Published: October 9, 2022

photothermal process.[10,12] Thus, the produced porous graphene structures possess a high conductivity and a high specific surface area (~340 m^2/g),[10] which are huge advantages for the improvement of MSCs.[13] Therefore, direct laser writing (DLW) represents a paradigm shift in the production of carbon-based electrodes for MSCs, as it is a rapid, simple, inexpensive, maskless, high-precision, and scalable technique resulting in virtually no waste being generated, thus being an environmentally friendly production method.[14,15]

Up to now, different native polymeric substrates have been used to produce these graphitic structures from synthetic polymers such as polyimide[6,16] or polysulfone[17] to natural materials such as wood,[18] cork,[19] and paper.[20,21] For instance, Tour and his team[6] transformed commercial polyimide films into porous graphene by simple laser induction, which was used for the fabrication of flexible, solid-state supercapacitors. Kulyk et al.[21] showed that by varying the lasing parameters, it is possible to improve the properties of LIG on paper, achieving sheet resistances of around 30 Ω/sq. The produced carbon material was then used to manufacture strain sensors. More recently, Pinheiro et al.[20] developed LIG on paper with a sheet resistance of 56 Ω/sq with very promising applications in biosensors. In fact, any carbon-based precursor substrate can in principle be converted to LIG. From the plethora of available substrates for LIG-based flexible technologies, parylene-C is one of the most interesting for device fabrication. It exhibits good mechanical properties, flexibility, biostability, and biocompatibility, which make it a favorable substrate for wearable, medical, and on-skin devices.[22] Moreover, parylene-C allows the production of ultrathin and conformable membranes and is compatible with standard microelectronics processing techniques while maintaining its biofriendly properties.[23] Thus, it has been widely used in several applications in biomedical, military, aerospace, and semiconductor industries, functioning as a flexible substrate,[24,25] as an encapsulation layer in electronic applications,[26] as a dielectric in chemical sensors,[27] or as a barrier to liquids and gases due to its low permeability.[23] However, LIG production on parylene-C has not been reported to date to the best of our knowledge.

In this work, we report, for the first time, a systematic study of the formation of LIG on parylene-C under CO_2 laser irradiation, followed by the fabrication of an in-plane, ultrathin MSC by an inexpensive, simple, and one-step approach. In more detail, we investigated the influence of different laser parameters in LIG synthesis, such as laser power, scan speed, atmosphere, and defocusing, on the resulting LIG morphology, structure, electrical conductivity, and chemical composition. By optimizing the laser parameters, a sheet resistance as low as 9.4 Ω/sq was obtained for LIG on parylene-C. The produced LIG MSC on parylene-C exhibited good electrochemical behavior, with an areal capacity of 1.66 mF/cm^2, a cycling stability of 96% after 10 000 cycles (0.5 mA/cm^2), and an energy density of 0.19 $\mu Wh/cm^2$ with a power density of 4.59 $\mu W/cm^2$. These results reinforce the potential of both parylene-C and LIG for cost-effective, biocompatible, and flexible energy-storage devices. This work allows one to further extend the knowledge of laser-induced graphene processes, widening the group of precursor substrates as well as promoting future applications.

2. MATERIALS AND METHODS

During this work, ultrapure laboratory-grade Milli-Q water (conductivity < 0.1 $\mu S/cm$) was used to prepare all solutions. Poly(vinyl alcohol) (PVA) and sulfuric acid were purchased from Sigma-Aldrich, and parylene-C (dimer of chloro-*para*-xylylene) was purchased from SCS—Specialty Coating Systems. All reagents were used as received, without further purification.

2.1. Parylene-C Deposition. Before deposition, glass substrates were cleaned in an ultrasonic bath at room temperature in acetone for 15 min, followed by the same treatment in isopropyl alcohol (IPA). Subsequently, the substrates were cleaned with deionized (DI) water and dried under N_2 flux, followed by annealing at 110 °C for 20 min in air. Afterward, a 5 wt % PVA solution was spin-coated onto the glass substrates at 1000 rpm for 10 s, followed by 2000 rpm for 20 s, and annealed at 110 °C for 2 min in air, forming a sacrificial layer for the peeling-off of the parylene-C membrane from the glass carrier at the end of the process. Finally, parylene-C deposition was carried out by a chemical vapor deposition (CVD) process using a commercially available deposition system PDS-2010 Labcoater 2 (Specialty Coating Systems). The thickness of the obtained films is controlled by the mass of the parylene-C dimer used and then verified in a profilometer. Thicknesses ranging from 10 to 13 μm were obtained using a dimer mass of around 20 g.

2.2. LIG Production. LIG production was carried out in a CO_2 laser cutting machine (VLS 3.50, Universal Laser Systems), with a wavelength of 10.6 μm, a beam size diameter of 0.127 mm, and a pulse of 1000 pulses per inch. All experiments were conducted at powers, speeds, and heights in the ranges of 2.5−4.5 W, 6.4−11.4 cm/s, and 0−1 mm above focus, respectively. LIG formation was studied under both air and nitrogen atmospheres. For security reasons, LIG was produced in a closed chamber with gas extraction.

2.3. LIG Characterization. The morphology of the produced LIG on parylene-C was evaluated by scanning electron microscopy (SEM) in a Carl Zeiss AURIGA CrossBeam FIB-SEM workstation equipped with an Oxford X-ray energy-dispersive spectrometer (Carl Zeiss Microscopy GmbH, Oberkochen, Germany) at an operating voltage of 5 keV under high vacuum. The electrical sheet resistance (R_{Sh}, Ω/sq) was determined by the Hall effect measurements in van der Pauw geometry (5 × 5 mm^2 architecture, with 1 mm circular silver conductive ink contacts at each corner) with a BioRad HL 5500 four-point probe equipment at room temperature. These measurements were performed in triplicate for each LIG sample. Room-temperature micro-Raman measurements were performed using a Horiba Jobin-Yvon HR800 spectrometer equipped with 600 grooves/mm grating, a 532 nm laser line (Ventus-LP-50085, Material Laser Quantum), and a 50 × objective (spot size ≈ 1.3 μm, NA = 0.5). Measurements were conducted with an exposure time of 10 s, 10 accumulations, and a laser power of 1.23 mW. To estimate the in-plane crystalline size from the ratio of the intensity of the G peak (I_G) and D peak (I_D) of the produced LIG, and its dependence on the growth conditions, the work of Cançado et al.[28] was used as a reference. Starting from the initial work of Tuinstra and Koenig,[29,30] these authors performed a detailed study on nanographite samples of different sizes with the purpose of establishing a relationship between the in-plane correlation size, L_a, independently measured by X-ray, and the Raman intensity ratio I_D/I_G, which was valid for any wavelength of excitation in the visible region. By this approach, they account for the dispersion behavior of the D band and reached the final empirical eq 1,[28] which was used in this work:

$$L_a = (2.4\times10^{-10}) \times \lambda_l^4 \times \left(\frac{I_G}{I_D}\right) \quad (1)$$

where λ_l is the wavelength of the excitation laser line (λ_l = 532 nm), and L_a represents an in-plane correlation length independently extracted from the Scherrer equation (after instrumental broadening correction), using the angle of the (100) diffraction peak measured with synchrotron radiation. Assuming the validity of the Scherrer equation, the in-plane correlation length, L_a, can represent the average in-plane crystalline size.

For X-ray photoelectron spectroscopy (XPS), a Kratos Axis Supra spectrometer equipped with a monochromatic Al Kα radiation source (1486.6 eV) was used.

https://doi.org/10.1021/acsami.2c09667
ACS Appl. Mater. Interfaces 2022, 14, 46427−46438

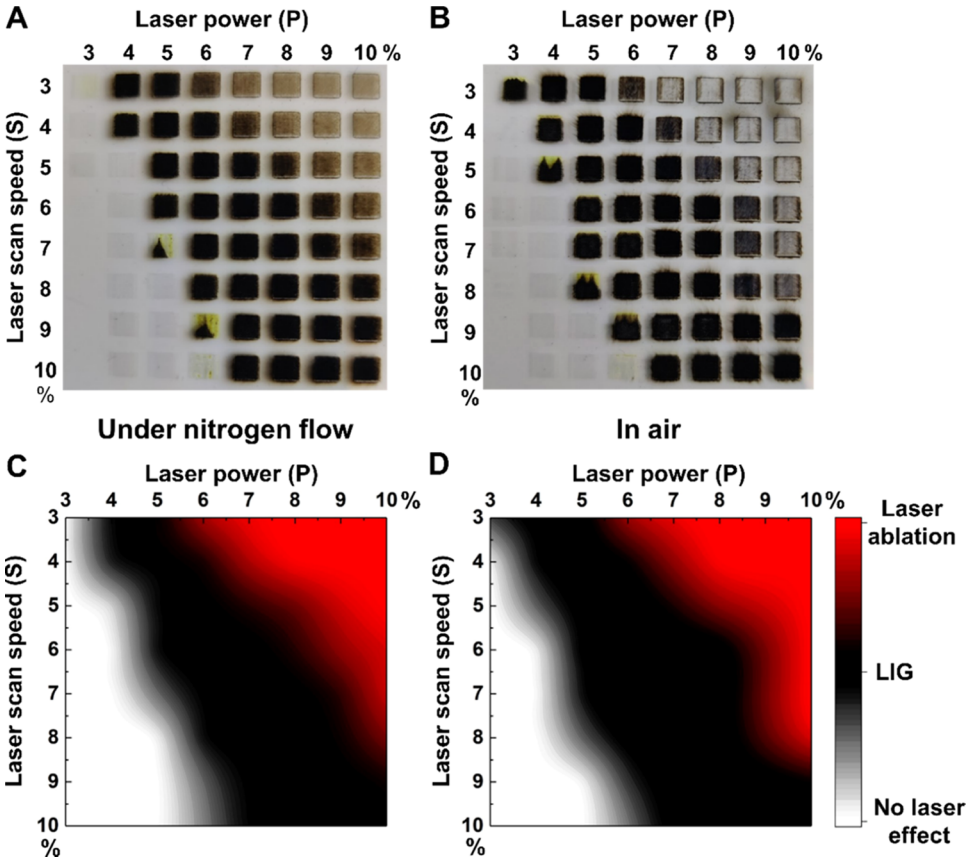

Figure 1. Images and corresponding heatmaps of the matrices formed by CO_2 laser irradiation on parylene-C (A, C) under nitrogen flow and (B, D) in air.

2.4. Parylene-C LIG Supercapacitor Fabrication. LIG interdigitated microsupercapacitor electrodes with an overall length of 1.9 cm, a width of 1.7 cm, an interspacing of 0.6 cm, and a line width of 0.8 cm were designed in an Adobe Illustrator and laser engraved onto parylene-C under optimized conditions. The pads of the current collector were coated with silver ink and cured for 1.5 h at 55 °C. A PVA/H_2SO_4 aqueous gel was used as the solid electrolyte. In a normal procedure, 1 g of PVA is dissolved in 10 mL of distilled water at 90 °C under vigorous stirring for 1 h. Then, 0.5 mL of 98% H_2SO_4 is added and allowed to mix for another hour. Before electrolyte casting, the MSCs were cured under UV light (NOVASCAN − PSD Pro Series•Digital UV Ozone System) to reduce the hydrophobicity of the LIG. The assembled MSCs were left to dry overnight at room temperature before the electrochemical testing. Finally, to obtain the flexible parylene-C LIG-MSC, the membrane needs to be peeled off from the glass substrate by dissolving the PVA sacrificial layer in water heated at 90 °C. However, this process must be conducted either before the electrolyte deposition or after a proper encapsulation of the device, which could be a parylene-C coating, to prevent the dissolution of the electrolyte in the heated water.

2.5. MSC Electrochemical Characterization. The electrochemical characterization of the produced LIG−MSC on parylene-C was conducted in a BioLogic SP-50 potentiostat (BioLogic Sciences Instruments) by means of cyclic voltammetry (5 mV/s to 10 V/s) and galvanostatic charge−discharge (0.010−1 mA/cm^2) experiments. Electrochemical impedance spectroscopy (5 mV, 1 MHz to 10 mHz) tests were carried out on a PalmSens 4.0 Potentiostat (PalmSens Compact Electrochemical Interfaces). The specific areal capacitance, C_A, values of the MSCs were calculated from the charge−discharge curves as follows:

$$C_A = \frac{I\Delta t}{A\Delta V} \tag{2}$$

where I is the applied current, Δt is the discharge time, and A is the MSC active area; $\Delta V = V_2 - V_1$, where V_2 is the potential at the beginning of discharge, after the internal resistance (IR) potential drop, and V_1 is the potential at the end of discharge. Energy (E_A) and power (P_A) per unit area were calculated as follows:

$$E_A = \frac{1}{2}\frac{C_A \Delta V^2}{3600} \tag{3}$$

$$P_A = \frac{3600 E_A}{\Delta t} \tag{4}$$

where 3600 is the conversion factor from Ws to Wh.

3. RESULTS AND DISCUSSION

3.1. Parylene-C LIG Formation and Characterization. *3.1.1. Laser Parameter Optimization for LIG Synthesis.* The innovative approach of LIG synthesis on parylene-C was carried out by varying four different laser working conditions, (i) laser power (P), (ii) laser scan speed (S), (iii) out-of-focus distances (D), and (iv) nitrogen flow (NF), to evaluate the ability of the laser to produce the graphitic material and optimize its quality. Therefore, a symmetric axis procedure was used for the study of the effects of the laser power and speed on LIG formation, as previously described by Pinheiro et al.,[20] at three different distances to the focal plane. Thus, P and S were varied from 3 to 10% of their maximum operational values (1.5−5 W and 3.8−12.7 cm/s, respectively). In this study, the considered distances in relation to the focal point were 0, 0.5, and 1 mm (above the focal point). The pulses per inch (ppi) were kept at a constant value of 1000 ppi.

https://doi.org/10.1021/acsami.2c09667
ACS Appl. Mater. Interfaces 2022, 14, 46427−46438

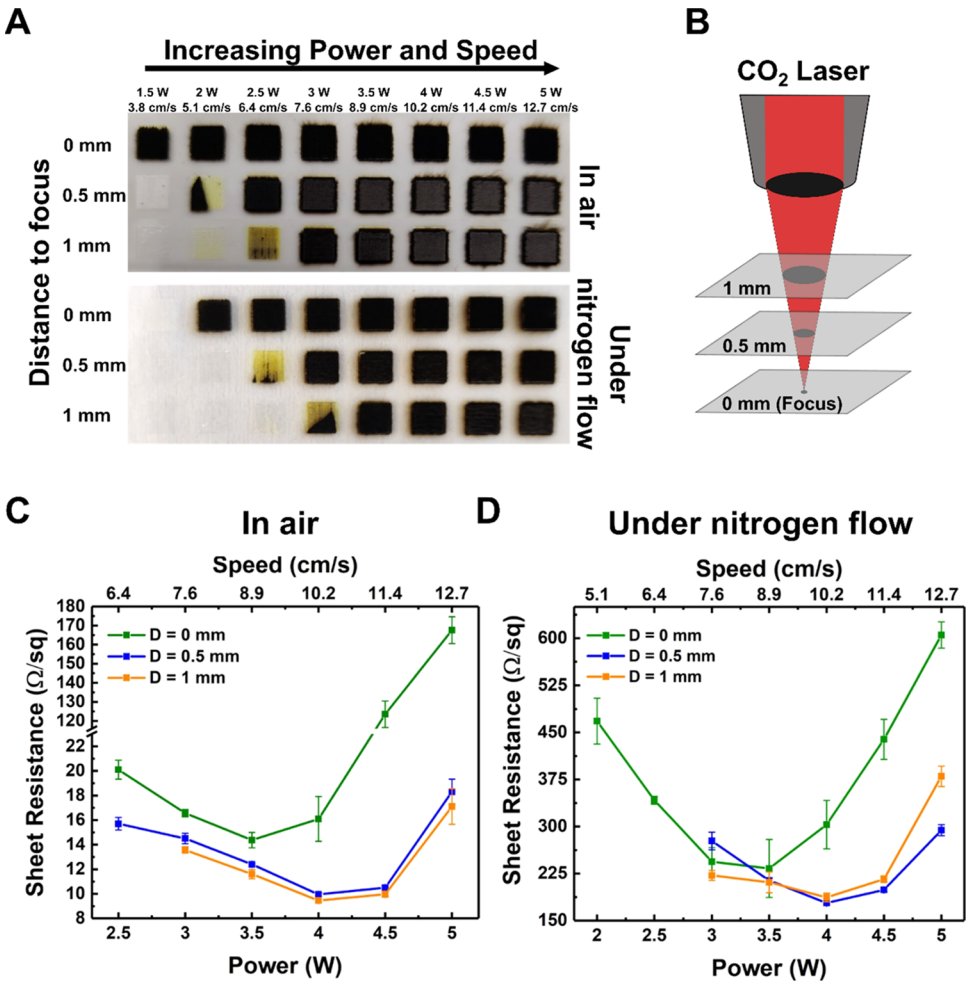

Figure 2. (A) LIG formation as a function of laser power, speed, and defocused distances in air and under nitrogen flow; (B) schematic of the defocused distances studied and corresponding sheet resistances obtained for LIG (C) in air and (D) under nitrogen flow.

Figure 1A,B displays the initial 8 × 8 matrices of power and speed coordinates, at the laser focal point (D = 0 mm), produced to evaluate the parameters that induce the synthesis of LIG under nitrogen flow or in air. For the sake of simplicity, percentage values of the laser power and speed are presented, and the correlation with the actual operational values is displayed in Table S1.

Generally, LIG formation can be visually inspected by the formation of darker samples when the precursor material is laser irradiated, as a consequence of its conversion to a graphite-based material.[12,20] It was observed that both matrices present an identical pattern. For lower percentage values of power relative to speed, the surface of parylene-C is modified, but the light color of the sample suggests that LIG is not formed, as the energy of the laser beam is not enough for graphene induction. On the other hand, in the high-power regime (power percentage values higher than speeds), the surface of parylene-C is destroyed. In this regimen, the differences between the presence and absence of nitrogen flow are evident, as the color of the produced samples changes from brown (under nitrogen flow) to silver (air). However, the formation of LIG seems to occur only for similar percentage values of power and speed, both in air and under nitrogen flow, where completely dark samples are visible, suggesting the production of the graphitic material. Specifically, darker samples were obtained for the symmetrical parameters, which generally represent a higher graphene induction, as shown in the heatmaps of the produced matrices (Figure 1C,D), and are in good agreement with the reports in the literature.[20] Therefore, this work will focus on these symmetrical conditions. Interestingly, for some samples, the formation of the graphitic material started at a single point further into the square, after which it expanded with each additional scan line, forming at the end a triangular shape, a phenomenon that was recently observed by Kulyk et al. for LIG synthesis on paper.[31]

To study the influence of laser defocusing on LIG induction, (5 × 5) mm^2 samples (Figure 2A,B) were produced at out-of-focus distances (0.5 and 1 mm above it) under symmetrical P and S conditions. As the distance above the focal point is increased, higher power is needed to induce the synthesis of LIG, either in air or under nitrogen flow, which was expected due to the spread of the laser beam and, consequently, less energy being provided by unit area. Furthermore, the samples produced out-of-focus exhibit good mechanical robustness as they do not tear apart during sample handling and testing, particularly the ones produced in air. It is not uncommon to obtain LIG as a powder, which renders it useless. In our case, the LIG is formed as a thin film, contributing to better mechanical properties. In particular, the samples produced out-of-focus in air present a dark-gray color with completely dark

https://doi.org/10.1021/acsami.2c09667
ACS Appl. Mater. Interfaces 2022, 14, 46427−46438

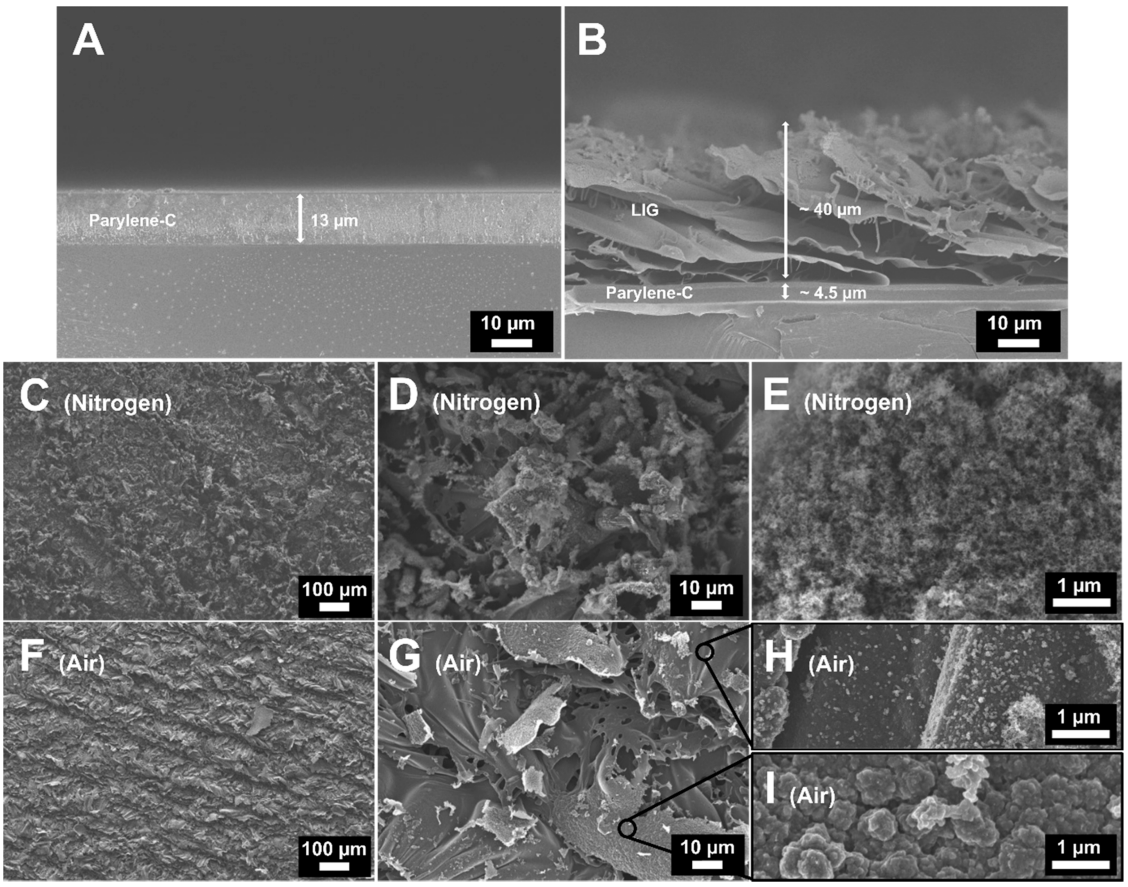

Figure 3. SEM cross-sectional micrographs of the parylene-C layer (A) before and (B) after laser irradiation at 4 W @ 10.2 cm/s in air. Top-view SEM micrographs of laser-induced graphene produced under nitrogen flow (C, D, E) and in air (F, G, H, I).

edges, suggesting different laser effects on the sample and on the borders, which is not the typical graphene pattern.

A better understanding of the influence of the laser parameters can be obtained by evaluating the electrical properties of the samples. Figure 2C,D presents the sheet resistance for the LIG-produced squares presented in Figure 2A. As observed, the absence of nitrogen flow strongly decreases the obtained sheet resistance, R_{Sh}, as the minimum value obtained with nitrogen flow (178.5 ± 1.7 Ω/sq) is still higher than the maximum value obtained in air (167.6 ± 6.9 Ω/sq). Thus, the presence of oxygen seems to be relevant in the synthesis of LIG in parylene-C. Moreover, it is evident that in both regimens, the samples produced out-of-focus present lower R_{Sh}; however, the difference between the out-of-focus distances of D = 0.5 mm and D = 1 mm is negligible. Furthermore, all curves present an identical behavior, where the initial R_{Sh} quickly decreases to an optimal value, and further increments on P and S result in an increase in R_{Sh}, suggesting sample deterioration. Interestingly, for LIG produced both in air and under nitrogen flow, the lowest value of sheet resistance is obtained when processed at 4 W and 10.2 cm/s with a defocused laser (D = 1 mm in air; D = 0.5 mm under nitrogen flow). In particular, the best results achieved were LIG produced in air at D = 1 mm, and an initial low R_{Sh} of 13.6 ± 0.3 Ω/sq (3 W @ 7.6 cm/s) decreases to a very low value of 9.4 ± 0.2 Ω/sq at a laser power of 4 W @ 10.2 cm/s, which is a remarkable achievement for an LIG-based material.[12,18,20,21] Moreover, as only a single laser irradiation is necessary to produce this highly conductive material, the whole synthesis process is very fast. This is a particularly important feature for the inexpensive upscaling of parylene-C LIG applications. An accurate comparison of LIG R_{Sh} across different systems is difficult to establish as the results are heavily dependent on the laser parameters and substrate used. However, to the best of our knowledge, the best R_{Sh} results reported for LIG-based materials are around 10 Ω/sq for polyimide[32] and 12 Ω/sq for coal,[33] which are similar to the values obtained in this work.

To further study the nature of the produced material, morphological, structural, and chemical characterization was conducted on LIG produced at 4 W @ 10.2 cm/s. Initially, before laser writing, parylene-C is a uniform flat layer without any observable or relevant features (Figures 3A and S1). However, the morphology radically changes upon laser irradiation in air, as the substrate seems to open cavities in its structure, which are composed of thin graphene sheets (Figure 3B−G). As we can observe, the produced sheet structure is well oriented in the same direction, which corresponds to the direction of the laser irradiation during the graphitization process. Moreover, LIG conversion is a subtractive process. The initial parylene-C layer exhibited a thickness of 13 μm, which was reduced to 4−5 μm due to its conversion to a graphene structure upon laser irradiation. On the other hand, the produced LIG structures showed a consistent thickness of around 40 μm. These results were similar without any relevant difference for both samples produced in air and under nitrogen flow. Furthermore, in the high-resolution micrographs, the sheets seem to present a

https://doi.org/10.1021/acsami.2c09667
ACS Appl. Mater. Interfaces 2022, 14, 46427−46438

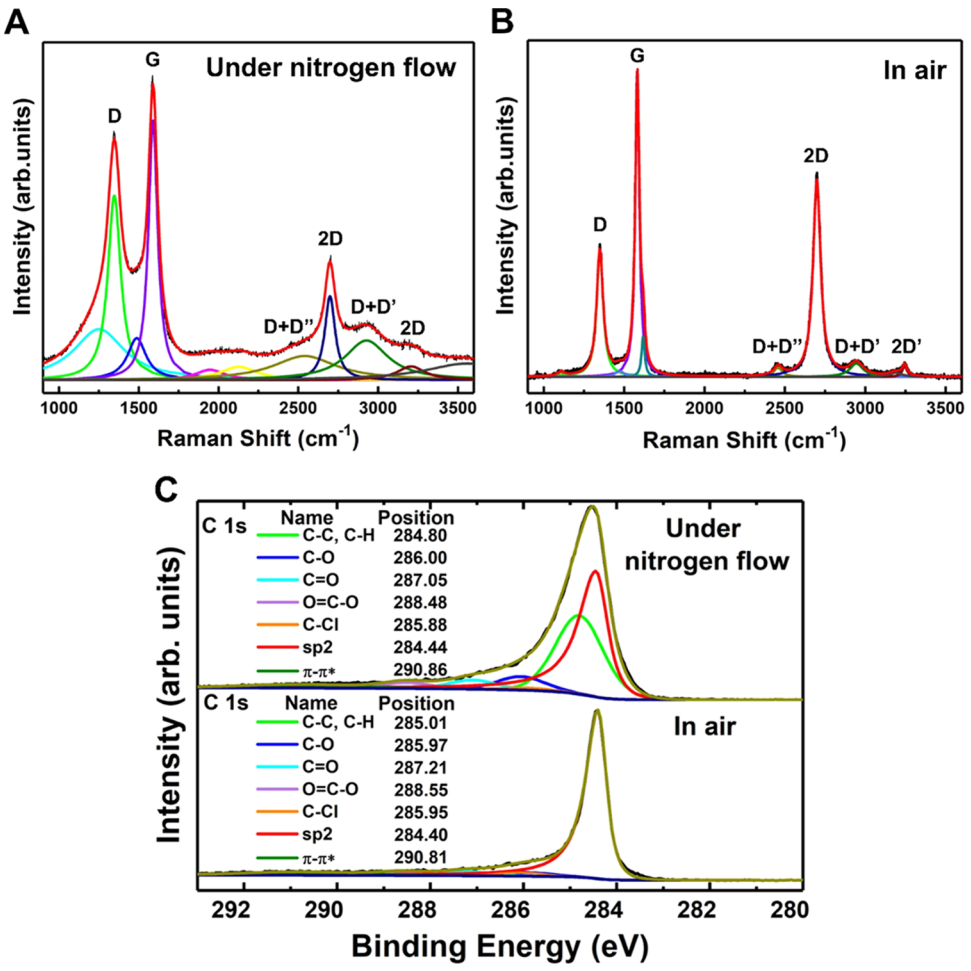

Figure 4. Representative Raman spectra of the optimized LIG samples (A) under nitrogen flow and (B) in air, and (C) the corresponding XPS spectra.

foamy graphene structure (Figure 3E,H). These porous structures are of high importance for MSC applications as they increase the available surface area and facilitate electrolyte penetration into the active materials.[12] Regarding the comparison between air and nitrogen flow LIG conditions, although the latter seems to present a higher porosity and lower pore size, the robustness of the carbon material is lower, as the LIG is barely attached to the surface and is easily removed during sample preparation and characterization. This is an undesirable effect for eventual LIG applications in wearable and flexible systems. On the other hand, LIG produced in air seems to overcome this problem as it is strongly attached to the parylene-C layer. In the Supporting Information, we present the morphological analysis of the evolution of the laser parameters tested in this work (1.5−5 W and 3.8−12.7 cm/s), in which it is easy to observe that progressive increments of the laser power and speed seem to increase the porosity of the resultant LIG, both under nitrogen flow (Figure S2) and in air (Figure S3). The increase in the porosity is directly associated with the liberation of gas from the photothermal conversion during the laser graphitization process. As the laser power increases, so does the gas release rate; consequently, the increased amount of gas released results in a larger pore distribution and higher porosity.[12,15]

Raman spectroscopy was conducted to evaluate the chemical structure of the produced LIG under optimized conditions (Figure 4A,B). As observed, both spectra present the three characteristic peaks of graphene-derived materials: first, the D peak around 1350 cm^{-1} is related to the breathing modes of six-atom rings and normally associated with the degree of defects in the sample as it requires a defect in its structure for its activation.[34] Afterward, the first-order G peak at around 1580 cm^{-1} is generated by graphitic carbon, and it is related to the bond stretching of sp^2 pairs in both carbon rings and chains.[34,35] Finally, the 2D peak at around 2700 cm^{-1} requires no defects for its activation as it originated from second-order zone-boundary phonons in a process where momentum conservation is achieved by two phonons with opposite wavevectors.[35,36] The intensity and symmetry of the 2D peak are the fingerprint signals of graphene.[35]

For both spectra, the defect-related D band presents high intensity, as expected, due to the high-density edges caused by the foamy nature of the material and the residual oxidation, which is characteristic of LIG.[12] In particular, the absence of the D′ band (~1620 cm^{-1}) suggests that the high edge density is the main contributor to the intense D band in opposition to structural defects.[37] However, the presence of typical D + D″, D + D′, and 2D′ broad bands is an indication of the defects in the material, which are typical of related graphene materials such as rGOs.[38,39] Moreover, for LIG produced both in air and under nitrogen flow, the 2D peak was fitted using only one Lorentzian curve at around 2700 cm^{-1}, which is the same

https://doi.org/10.1021/acsami.2c09667
ACS Appl. Mater. Interfaces 2022, 14, 46427−46438

procedure used for single-layer graphene,[36] thus suggesting that the produced LIG is far from the graphitic form. However, the full width at half-maximum (FWHM) is ∼57 cm^{-1} for LIG in air and ∼78 cm^{-1} for LIG under nitrogen, which is larger than the values measured in single-layer graphene (∼30 cm^{-1}).[36,40−42] Therefore, the 2D band profile obtained under both conditions is commonly found in 2D graphite materials composed of randomly stacked graphene layers along the *c* axis, as it is normally verified for LIG samples.[43,44] However, the differences between the two spectra are evident. First, LIG prepared in air (Figure 4B) presents a lower signal/noise ratio and the peaks are sharper and narrower, indicating higher graphene quality, as the FWHM values for these samples are ∼48 cm^{-1} for the D-band, ∼31 cm^{-1} for the G-band, and ∼57 cm^{-1} for the 2D-band, whereas for the samples fabricated under nitrogen (Figure 4A), the FWHM noticeably increased to ∼98, ∼140, and ∼78 cm^{-1}, respectively. Moreover, analyzing the I_D/I_G ratios of 0.42 (LIG in air) vs 0.71 (LIG under nitrogen flow), the comparatively lower ratio of LIG produced in air translates to fewer defects in the graphene structure,[36] in good agreement with the lower sheet resistance measured. In addition, the I_D/I_G ratio allows us to determine the crystallite size along the *a* axis (L_a) using eq 4 (Sections 2−2.3). The increase in the crystallite size from ∼27 nm (LIG under nitrogen flow) to ∼46 nm (LIG in air) suggests that high surface temperatures during graphene formation promote larger graphene regions[12,45] and, consequently, reduce the presence of lateral defects.[46] Furthermore, the I_{2D}/I_G ratio of 0.65 for LIG produced in air vs 0.32 for LIG under nitrogen flow (both <1, as commonly observed for LIG) is also a good indication of the higher quality of the former because a higher intensity of the 2D peak is an important characteristic of the quality of graphene.[47] This ratio can also give an estimation of the number of graphene layers, which will be lower for higher I_{2D}/I_G ratios (>2 for single-layered graphene), indicating that LIG produced both in air and under nitrogen flow are expected to be composed of few-layered graphene sheets, with the former presenting a smaller number of layers.[47,48]

To corroborate the Raman structural characterization, the chemical and elemental composition of parylene-C LIG was assessed by X-ray photoelectron spectroscopy (XPS). The full XPS survey spectrum of parylene-C LIG is shown in Figure S4A, whereas the C 1s spectrum of the parylene-C substrate is displayed in Figure S4B. Figure 4C compares the C 1s spectra of LIG produced under nitrogen flow and in air, with the deconvolution of the spectra into six peaks: C═C (sp^2 at 284.4 eV), C−C (sp^3), C−O, C═O, O═C−O, C−Cl, and $\pi-\pi^*$; these results are in good agreement with other studies reported in the literature.[18,21,49] As observed, both spectra are dominated by the sp^2 carbon peak, characteristic of graphitic materials, in opposition to the C−C (sp^3) bond, confirming the graphitization process and the formation of LIG structures in the laser-irradiated parylene-C films. Interestingly, the sample under ambient conditions exhibits less oxygen functional groups, thus suggesting that inert or less oxidative atmospheres may be detrimental to LIG production. In fact, in terms of the robustness of fabrication, sheet resistance, and chemical structure, LIG produced in air presents better quality than LIG produced under nitrogen flow, a phenomenon that was also reported by Mamleyev et al.[50] for polyimide substrates. Other reports indicate that LIG properties are enhanced under inert atmospheres as undesired oxidation side reactions during the pyrolysis and carbonization processes can be avoided.[51−53] In fact, the atmospheric composition has been verified as a key parameter for LIG processing.[13] For instance, the LIG surface can be made superhydrophilic or superhydrophobic by processing the precursor material under O_2/air or in an inert atmosphere, respectively.[54] Atmospheres richer in oxygen result in the formation of LIG containing more oxygen atoms; thus, it becomes easier for edges to come in contact with water, rendering the surfaces more hydrophilic. However, the influence of the atmosphere during the lasing process on the structural, morphological, electrical, and physicochemical properties of the produced LIG material remains a topic that still needs further research. Therefore, as there is no conclusive opinion on these matters, further LIG production on parylene will be pursued under the better conditions described in this paper.

Table 1 shows a literature overview of the electrical and chemical properties obtained by laser engraving of different substrates to establish a comparison between the obtained results of this work and LIG obtained from various polymeric and composite materials. As observed, the electrical results (R_{Sh}) for LIG on parylene-C are in line with the values reported for other commonly used polymeric substrates, such as PI. A similar result can be observed for the chemical properties of parylene-C-based LIG, as the obtained Raman I_D/I_G and I_{2D}/I_G ratios and crystallite sizes are similar to values reported in the literature. Again, Table 1 also suggests that working in air promotes the overall LIG properties.

Table 1. Comparison of Electrical and Chemical Properties of LIG Produced from Different Substrates

substrate	atmosphere	R_{Sh} (Ω/sq)	I_D/I_G	L_a (nm)	I_{2D}/I_G	ref
coal	air	12	0.78	n.a.	0.92	33
cork	air	75	0.41	22	0.37	19
cork	air	46	1.00	n.a.	0.37	55
paper (filter)	air	32	0.50	n.a.	n.a.	21
paper (Whatman)	nitrogen	56	1.28	n.a.	0.62	20
paper (office)	nitrogen	217.7	1.33	n.a.	0.27	20
KL/PEO	air	363.1	0.50	19	0.40	56
PEI	air	15	n.a.	n.a.	n.a.	57
PI	air	15	0.44	32	0.88	12
PI	air	9.3	n.a.	n.a.	n.a.	32
PI	air	29.1	0.80	24	n.a.	50
PI	nitrogen	n.a.	1.10	17	n.a.	50
PI/PDMS	n.a.	80	0.72	23	0.61	58
wood	Ar/H_2	10	0.85	20	0.55	18
parylene-C	air	9.4	0.42	46	0.65	this work
parylene-C	nitrogen	178.5	0.71	27	0.32	this work

So far, LIG in different substrates has been implemented in several devices, namely sensors,[16,39,59,60] energy-storage devices,[61−63] and conductive tracks for flexible circuits.[64] The low sheet resistance and apparent porous/open structure of LIG produced in parylene suggest that it could be used for MSC fabrication. Usually, these devices benefit from porous and conductive materials that enhance the electrochemical response.[5,7] In the following section, we study this possibility by fabricating an interdigitated MSC on parylene by DLW, as a proof of concept.

https://doi.org/10.1021/acsami.2c09667
ACS Appl. Mater. Interfaces 2022, 14, 46427−46438

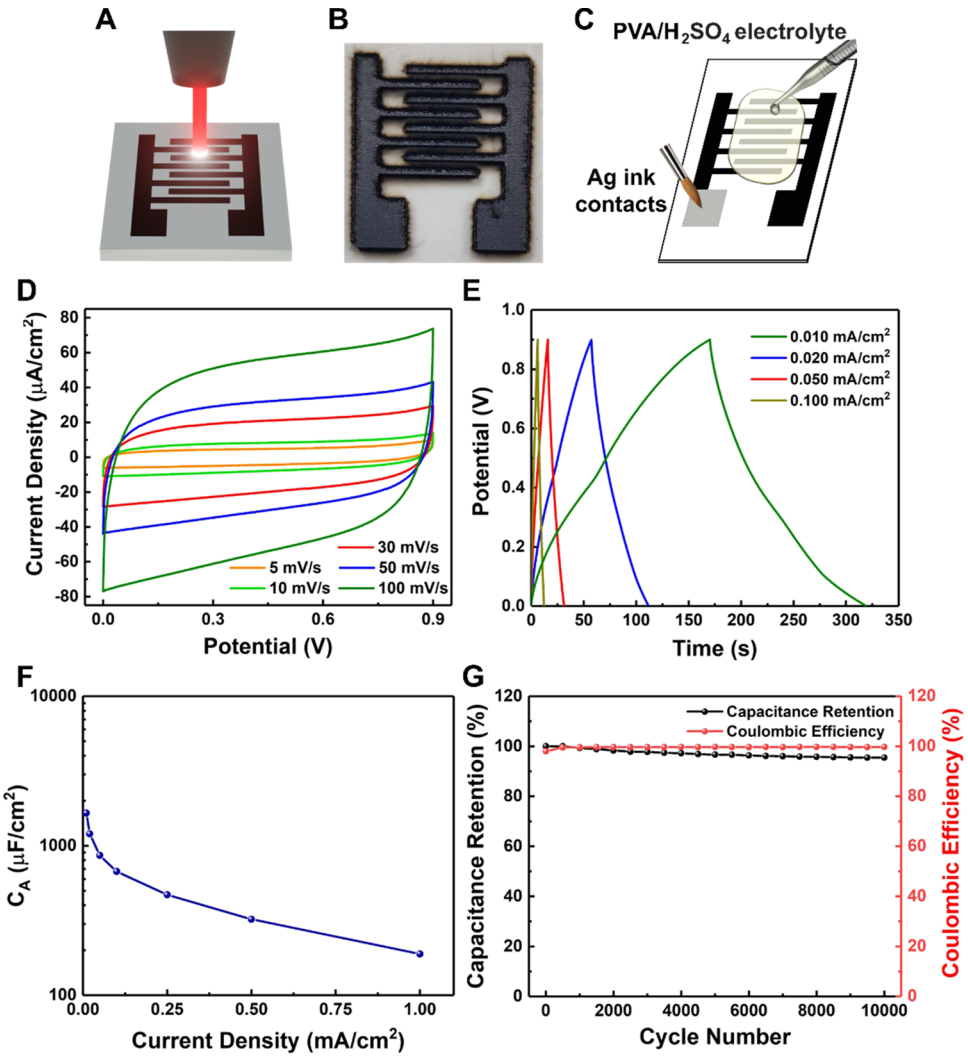

Figure 5. (A) Direct laser-writing process; (B) LIG−MSC electrodes directly written on a parylene-C film; (C) schematics of the LIG−MSC assembly; (D) cyclic voltammetry, (E) charge−discharge curves, (F) capacitance at different current densities, and (G) capacitance retention and Coulombic efficiency at 0.5 mA/cm^2 for LIG−MSC on parylene-C.

3.2. MSC Fabrication and Electrochemical Characterization. The quality of the parylene-C LIG produced, coupled with its good electrical properties, makes it highly attractive for applications in energy-storage systems. Thus, we fabricated interdigitated in-plane MSCs, under the optimized LIG parameters (4 W @ 10.2 cm/s @ 1 mm above focus, in air), in which the LIG worked as both the current collector and the active material in an electrical double-layered structure. Figure 5A demonstrates the process of laser irradiation, and Figure 5B shows the well-defined LIG-MSC electrodes directly written on parylene-C sheets with an interfinger distance of ∼600 μm. These devices present a fine architecture, comparable to other reported MSCs. However, LIG-MSCs were produced by a one-step approach by a potentially scalable method. In comparison with other techniques, such as printing[65,66] and stamping,[67,68] LIG does not require complicated multistep processes. In addition, as a digital method, it is quite simple to change the device format or architecture by laser engraving. After the devices are prepared, silver ink was applied to the electrodes to create electrical contacts (Figures 5C and S5). Moreover, PVA/H_2SO_4 was used as the electrolyte, and the electrochemical and energy-storage properties were characterized by cyclic voltammetry (CV) and galvanostatic charge−discharge (GCD) experiments.

Figure 5D shows the CV curves of the produced MSC (5−100 mV/s). Despite the presence of oxygen in the produced LIG, the quasirectangular shape of the curves with no anodic and cathodic peaks indicates good electrochemical performance and is characteristic of electric double-layered capacitors (EDLCs).[69,70] Even with an increase in the scan rate up to 500 mV/s (shown in Figure S7), the quasirectangular shape is maintained, which again indicates the good electrochemical stability and the possibility of high-power performance. A similar indication of the good capacitive behavior can be obtained by the GCD curves shown in Figure 5E, as they exhibit an almost ideal symmetric triangular shape and a very low voltage drop. Moreover, an areal capacitance (C_A) of 1.66 ± 0.41 mF/cm^2 was obtained for a current density of 0.010 mA/cm^2 (Figure 5F), which is in line with other previously reported studies.[71] Under similar conditions, Tour et al.[12] obtained 5 mF/cm^2 on polyimide (PI), whereas Shi and coworkers[72] obtained 0.62 mF/cm^2 on a PI substrate, thus indicating a significant capacitance variation across similar systems, which again makes it difficult to compare the different reported MSCs. In addition, as previously shown in Figure 3B,

https://doi.org/10.1021/acsami.2c09667
ACS Appl. Mater. Interfaces 2022, 14, 46427−46438

the produced LIG layer is very thin (less than 50 μm). Therefore, the obtained specific capacitance should in principle be lower than the values obtained for thicker and porous substrates such as paper[73,74] and other cellulose-based materials,[55,75−77] for instance. Moreover, higher capacitances have also been obtained for doped graphene/LIG electrodes[78,79] or systems prepared by more complicated or expensive methods.[8,80] Nevertheless, the specific capacitance achieved represents a good result considering the lower LIG thickness and undoped nature. In addition, the cycling performance shows that the produced devices can retain 96% of their initial capacitance after 10 000 cycles at 0.50 mA/cm^2, revealing very low capacity loss (Figure 5G). In addition, the Coulombic efficiency is maintained at 99.7% after 10 000 cycles (Figure 5G). Finally, in terms of energy density, the LIG-MSC exhibits 0.19 μWh/cm^2 with a power density of 4.59 μW/cm^2. Additional electrochemical analyses and discussion can be found in the Supporting Information.

The present work describes LIG fabrication on parylene-C and its possible application in energy-storage applications. As previously described, parylene is usually used as a coating for many applications. Therefore, this work indicates the potential of parylene-C-based LIG devices, combining the good electrical and chemical properties with the renowned biocompatibility of the films. To obtain a flexible and conformable parylene-C LIG membrane, the thin film needs to be peeled off from the glass substrate. Figure S6 shows the thin parylene-C LIG membrane after the peeling-off process. As observed, the produced LIG parylene-C film maintains its robustness as LIG appears to not be affected by the process. Further studies will be conducted to better understand the mechanical properties of the produced LIG and MSC, aiming at expanding its applications.

4. CONCLUSIONS

In this work, the formation of LIG on parylene-C sheets using CO_2 laser irradiation by a simple, one-step, scalable, and cost-effective approach was systematically studied. In particular, the influence of different processing parameters, such as the laser power, scan speed, atmosphere, and defocusing, on the produced LIG structures has been explored. By optimizing the laser parameters (4 W @ 10.2 cm/s, in air), sheet resistances as low as 9.4 Ω/sq were obtained for the produced LIG. Thus, the resulting physical and chemical properties of the obtained LIG material endow them with suitable properties for implementation in flexible technologies as energy-storage devices with promising electrochemical performance. In this context, as a proof of concept, LIG-based MSCs on parylene-C were fabricated in an interdigitated configuration, with LIG working as both the current collector and the active material. The assembled MSC exhibited good electrochemical behavior, with an areal capacity of 1.66 mF/cm^2 and a cycling stability of 96% after 10 000 cycles (0.5 mA/cm^2). These results expand our knowledge of LIG processes and allow further development of flexible, portable, and biocompatible electronic devices with parylene-C LIG for environmentally friendly and cost-effective applications.

■ ASSOCIATED CONTENT

Supporting Information

The Supporting Information is available free of charge at https://pubs.acs.org/doi/10.1021/acsami.2c09667.

Laser power parameters; interface and cross-sectional SEM micrographs of parylene-C LIG; SEM micrographs of LIG produced under nitrogen flow; SEM micrographs of LIG produced in air; XPS LIG characterization; photograph of the produced LIG MSC device; images of the produced LIG electrodes on parylene-C after peeling-off; LIG MSC cyclic voltammetry characterization; LIG MSC Nyquist plot (PDF)

■ AUTHOR INFORMATION

Corresponding Authors

Ricardo Correia − *CENIMAT|i3N Department of Materials Science, NOVA School of Science and Technology and CEMOP/UNINOVA, 2829-516 Caparica, Portugal;* orcid.org/0000-0001-9285-3569; Email: rfe.correia@campus.fct.unl.pt

João Coelho − *CENIMAT|i3N Department of Materials Science, NOVA School of Science and Technology and CEMOP/UNINOVA, 2829-516 Caparica, Portugal;* orcid.org/0000-0003-4217-3842; Email: jcm.coelho@fct.unl.pt

Rodrigo Martins − *CENIMAT|i3N Department of Materials Science, NOVA School of Science and Technology and CEMOP/UNINOVA, 2829-516 Caparica, Portugal;* Email: rm@uninova.pt

Authors

Jonas Deuermeier − *CENIMAT|i3N Department of Materials Science, NOVA School of Science and Technology and CEMOP/UNINOVA, 2829-516 Caparica, Portugal;* orcid.org/0000-0002-2764-3124

Maria Rosário Correia − *i3N-Aveiro, Physics Department, University of Aveiro, 3810-193 Aveiro, Portugal;* orcid.org/0000-0003-3781-0085

Joana Vaz Pinto − *CENIMAT|i3N Department of Materials Science, NOVA School of Science and Technology and CEMOP/UNINOVA, 2829-516 Caparica, Portugal;* orcid.org/0000-0003-0847-7711

Elvira Fortunato − *CENIMAT|i3N Department of Materials Science, NOVA School of Science and Technology and CEMOP/UNINOVA, 2829-516 Caparica, Portugal;* orcid.org/0000-0002-4202-7047

Complete contact information is available at: https://pubs.acs.org/10.1021/acsami.2c09667

Author Contributions

This manuscript was written through contributions of all authors. All authors have given approval to the final version of the manuscript.

Notes

The authors declare no competing financial interest.

■ ACKNOWLEDGMENTS

This work was financed by national funds from FCT - Fundação para a Ciência e a Tecnologia, I.P., in the scope of the projects LA/P/0037/2020, UIDP/50025/2020, and UIDB/50025/2020 of the Associate Laboratory Institute of Nanostructures, Nanomodelling, and Nanofabrication − i3N. Moreover, the authors acknowledge the ERC AdG project DIGISMART ref 787410 and EC project SYNERGY H2020-WIDESPREAF-2020-5, CSA, proposal number 952169. R.C. acknowledges funding from i3N-FCT I.P. through the PhD

Grant UI/BD/151295/2021. The authors thank Dr. Emanuel Carlos for SEM image acquisition.

■ ABBREVIATIONS

LIG, laser-induced graphene
MSC, microsupercapacitors
DLW, direct laser writing
PVA, poly(vinyl alcohol)
SEM, scanning electron microscopy
XPS, X-ray photoelectron spectroscopy
P, laser power
S, laser scan speed
D, out-of-focus distance
R_{Sh}, sheet resistance
CV, cyclic voltammetry
GCD, galvanostatic charge−discharge

■ REFERENCES

(1) Palchoudhury, S.; Ramasamy, K.; Gupta, R. K.; Gupta, A. Flexible Supercapacitors: A Materials Perspective. *Front. Mater.* **2019**, *5*, No. 83.
(2) Hota, M. K.; Jiang, Q.; Wang, Z.; Wang, Z. L.; Salama, K. N.; Alshareef, H. N. Integration of Electrochemical Microsupercapacitors with Thin Film Electronics for On-Chip Energy Storage. *Adv. Mater.* **2019**, *31*, No. 1807450.
(3) Muralee Gopi, C. V. V.; Vinodh, R.; Sambasivam, S.; Obaidat, I. M.; Kim, H. J. Recent Progress of Advanced Energy Storage Materials for Flexible and Wearable Supercapacitor: From Design and Development to Applications. *J. Energy Storage* **2020**, *27*, No. 101035.
(4) Coelho, J.; Kremer, M. P.; Pinilla, S.; Nicolosi, V. An Outlook on Printed Microsupercapacitors: Technology Status, Remaining Challenges, and Opportunities. *Curr. Opin. Electrochem.* **2020**, *21*, 69−75.
(5) Kyerematen, N. A.; Brousse, T.; Pech, D. Microsupercapacitors as Miniaturized Energy-Storage Components for on-Chip Electronics. *Nat. Nanotechnol.* **2017**, *12*, 7−15.
(6) Peng, Z.; Lin, J.; Ye, R.; Samuel, E. L. G.; Tour, J. M. Flexible and Stackable Laser-Induced Graphene Supercapacitors. *ACS Appl. Mater. Interfaces* **2015**, *7*, 3414−3419.
(7) Liang, J.; Mondal, A. K.; Wang, D. W.; Iacopi, F. Graphene-Based Planar Microsupercapacitors: Recent Advances and Future Challenges. *Adv. Mater. Technol.* **2019**, *4*, No. 1800200.
(8) Zhang, P.; Wang, F.; Yu, M.; Zhuang, X.; Feng, X. Two-Dimensional Materials for Miniaturized Energy Storage Devices: From Individual Devices to Smart Integrated Systems. *Chem. Soc. Rev.* **2018**, *47*, 7426−7451.
(9) Sun, Y.; Wu, Q.; Shi, G. Graphene Based New Energy Materials. *Energy Environ. Sci.* **2011**, *4*, 1113−1132.
(10) Ye, R.; James, D. K.; Tour, J. M. Laser-Induced Graphene. *Acc. Chem. Res.* **2018**, *51*, 1609−1620.
(11) Chyan, Y.; Cohen, J.; Wang, W.; Zhang, C.; Tour, J. M. Graphene Art. *ACS Appl. Nano Mater.* **2019**, *2*, 3007−3011.
(12) Lin, J.; Peng, Z.; Liu, Y.; Ruiz-Zepeda, F.; Ye, R.; Samuel, E. L. G.; Yacaman, M. J.; Yakobson, B. I.; Tour, J. M. Laser-Induced Porous Graphene Films from Commercial Polymers. *Nat. Commun.* **2014**, *5*, No. 5714.
(13) Ma, W.; Zhu, J.; Wang, Z.; Song, W.; Cao, G. Recent Advances in Preparation and Application of Laser-Induced Graphene in Energy Storage Devices. *Mater. Today Energy* **2020**, *18*, No. 100569.
(14) Duy, L. X.; Peng, Z.; Li, Y.; Zhang, J.; Ji, Y.; Tour, J. M. Laser-Induced Graphene Fibers. *Carbon* **2018**, *126*, 472−479.
(15) Ye, R.; James, D. K.; Tour, J. M. Laser-Induced Graphene: From Discovery to Translation. *Adv. Mater.* **2019**, *31*, No. 1803621.
(16) Samouco, A.; Marques, A. C.; Pimentel, A.; Martins, R.; Fortunato, E. Laser-Induced Electrodes towards Low-Cost Flexible UV ZnO Sensors. *Flexible Printed Electron.* **2018**, *3*, No. 044002.
(17) Mishra, N. K.; Patil, N.; Anas, M.; Zhao, X.; Wilhite, B. A.; Green, M. J. Highly Selective Laser-Induced Graphene (LIG)/Polysulfone Composite Membrane for Hydrogen Purification. *Appl. Mater. Today* **2021**, *22*, No. 100971.
(18) Ye, R.; Chyan, Y.; Zhang, J.; Li, Y.; Han, X.; Kittrell, C.; Tour, J. M. Laser-Induced Graphene Formation on Wood. *Adv. Mater.* **2017**, *29*, No. 1702211.
(19) Carvalho, A. F.; Fernandes, A. J. S.; Martins, R.; Fortunato, E.; Costa, F. M. Laser-Induced Graphene Piezoresistive Sensors Synthesized Directly on Cork Insoles for Gait Analysis. *Adv. Mater. Technol.* **2020**, *5*, No. 2000630.
(20) Pinheiro, T.; Silvestre, S.; Coelho, J.; Marques, A. C.; Martins, R.; Sales, M. G. F.; Fortunato, E. Laser-Induced Graphene on Paper toward Efficient Fabrication of Flexible, Planar Electrodes for Electrochemical Sensing. *Adv. Mater. Interfaces* **2021**, *8*, No. 2101502.
(21) Kulyk, B.; Silva, B. F. R.; Carvalho, A. F.; Silvestre, S.; Fernandes, A. J. S.; Martins, R.; Fortunato, E.; Costa, F. M. Laser-Induced Graphene from Paper for Mechanical Sensing. *ACS Appl. Mater. Interfaces* **2021**, *13*, 10210−10221.
(22) Golda-Cepa, M.; Engvall, K.; Hakkarainen, M.; Kotarba, A. Recent Progress on Parylene C Polymer for Biomedical Applications: A Review. *Prog. Org. Coat.* **2020**, *140*, No. 105493.
(23) Ortigoza-Diaz, J.; Scholten, K.; Larson, C.; Cobo, A.; Hudson, T.; Yoo, J.; Baldwin, A.; Hirschberg, A. W.; Meng, E. Techniques and Considerations in the Microfabrication of Parylene C Microelectromechanical Systems. *Micromachines* **2018**, *9*, No. 422.
(24) Wang, Y.; Dai, W.; Wu, Y.; Guo, Y.; Xu, R.; Yan, B.; Xu, Y. In *A Bendable Microwave GaN HEMT on CVD Parylene-C Substrate*, 2020 IEEE MTT-S International Conference on Numerical Electromagnetic and Multiphysics Modeling and Optimization, NEMO 2020; IEEE, 2020.
(25) Neto, J. P.; Costa, A.; Vaz Pinto, J.; Marques-Smith, A.; Costa, J. C.; Martins, R.; Fortunato, E.; Kampff, A. R.; Barquinha, P. Transparent and Flexible Electrocorticography Electrode Arrays Based on Silver Nanowire Networks for Neural Recordings. *ACS Appl. Nano Mater.* **2021**, *4*, 5737−5747.
(26) Kiazadeh, A.; Gomes, H. L.; Barquinha, P.; Martins, J.; Rovisco, A.; Pinto, J.; Martins, R.; Fortunato, E. Improving Positive and Negative Bias Illumination Stress Stability in Parylene Passivated IGZO Transistors. *Appl. Phys. Lett.* **2016**, *109*, No. 051606.
(27) Veigas, B.; Pinto, J.; Vinhas, R.; Calmeiro, T.; Martins, R.; Fortunato, E.; Baptista, P. V. Quantitative Real-Time Monitoring of RCA Amplification of Cancer Biomarkers Mediated by a Flexible Ion Sensitive Platform. *Biosens. Bioelectron.* **2017**, *91*, 788−795.
(28) Cançado, L. G.; Takai, K.; Enoki, T.; et al. General Equation for the Determination of the Crystallite Size La of Nanographite by Raman Spectroscopy. *Appl. Phys. Lett.* **2006**, *88*, No. 163106.
(29) Tuinstra, F.; Koenig, J. L. Raman Spectrum of Graphite. *J. Chem. Phys.* **1970**, *53*, 1126−1130.
(30) Knight, D. S.; White, W. B. Characterization of Diamond Films by Raman Spectroscopy. *J. Mater. Res.* **2011**, *4*, 385−393.
(31) Kulyk, B.; Silva, B. F. R.; Carvalho, A. F.; Barbosa, P.; Girão, A.; Deuermeier, J.; Fernandes, A. J. S.; Figueiredo, F. M. L.; Fortunato, E.; Costa, F. M. Laser-Induced Graphene from Paper by Ultraviolet Irradiation: Humidity and Temperature Sensors. *Adv. Mater. Technol.* **2022**, *7*, No. 2101311.
(32) Li, X.; Cai, W.; Teh, K. S.; Qi, M.; Zang, X.; Ding, X.; Cui, Y.; Xie, Y.; Wu, Y.; Ma, H.; Zhou, Z.; Huang, Q. A.; Ye, J.; Lin, L. High-Voltage Flexible Microsupercapacitors Based on Laser-Induced Graphene. *ACS Appl. Mater. Interfaces* **2018**, *10*, 26357−26364.
(33) Zhang, C.; Xie, Y.; Zhang, C.; Lin, J. Upgrading Coal to Multifunctional Graphene Based Materials by Direct Laser Scribing. *Carbon* **2019**, *153*, 585−591.
(34) Malard, L. M.; Pimenta, M. A.; Dresselhaus, G.; Dresselhaus, M. S. Raman Spectroscopy in Graphene. *Phys. Rep.* **2009**, *473*, 51−87.
(35) Ferrari, A. C.; Basko, D. M. Raman Spectroscopy as a Versatile Tool for Studying the Properties of Graphene. *Nat. Nanotechnol.* **2013**, *8*, 235−246.
(36) Ferrari, A. C.; Meyer, J. C.; Scardaci, V.; Casiraghi, C.; Lazzeri, M.; Mauri, F.; Piscanec, S.; Jiang, D.; Novoselov, K. S.; Roth, S.;

https://doi.org/10.1021/acsami.2c09667
ACS Appl. Mater. Interfaces 2022, 14, 46427−46438

Geim, A. K. Raman Spectrum of Graphene and Graphene Layers. *Phys. Rev. Lett.* **2006**, *97*, No. 187401.
(37) Eckmann, A.; Felten, A.; Mishchenko, A.; Britnell, L.; Krupke, R.; Novoselov, K. S.; Casiraghi, C. Probing the Nature of Defects in Graphene by Raman Spectroscopy. *Nano Lett.* **2012**, *12*, 3925−3930.
(38) Muhammad Hafiz, S.; Ritikos, R.; Whitcher, T. J.; Md Razib, N.; Bien, D. C. S.; Chanlek, N.; Nakajima, H.; Saisopa, T.; Songsiriritthigul, P.; Huang, N. M.; Rahman, S. A. A Practical Carbon Dioxide Gas Sensor Using Room-Temperature Hydrogen Plasma Reduced Graphene Oxide. *Sens. Actuators, B* **2014**, *193*, 692−700.
(39) Carvalho, A. F.; Fernandes, A. J. S.; Leitão, C.; Deuermeier, J.; Marques, A. C.; Martins, R.; Fortunato, E.; Costa, F. M. Laser-Induced Graphene Strain Sensors Produced by Ultraviolet Irradiation of Polyimide. *Adv. Funct. Mater.* **2018**, *28*, No. 1805271.
(40) Kattel, S.; Scougale, W. R.; Murphy, J. R.; Pasco, S. R.; Ackerman, J.; Alvarado, V.; Rice, W. D. Spectroscopic Determination of Ice-Induced Interfacial Strain on Single-Layer Graphene. *Small* **2020**, *16*, No. 2003892.
(41) Tao, Z.; Du, J.; Qi, Z.; Ni, K.; Jiang, S.; Zhu, Y. Raman Spectroscopy Study of Sp2 to Sp3 Transition in Bilayer Graphene under High Pressures. *Appl. Phys. Lett.* **2020**, *116*, No. 133101.
(42) Kim, K.; Coh, S.; Tan, L. Z.; Regan, W.; Yuk, J. M.; Chatterjee, E.; Crommie, M. F.; Cohen, M. L.; Louie, S. G.; Zettl, A. Raman Spectroscopy Study of Rotated Double-Layer Graphene: Misorientation-Angle Dependence of Electronic Structure. *Phys. Rev. Lett.* **2012**, *108*, No. 246103.
(43) Cançado, L. G.; Pimenta, M. A.; Saito, R.; Jorio, A.; Ladeira, L. O.; Grueneis, A.; Souza-Filho, A. G.; Dresselhaus, G.; Dresselhaus, M. S. Stokes and Anti-Stokes Double Resonance Raman Scattering in Two-Dimensional Graphite. *Phys. Rev. B* **2002**, *66*, No. 035415.
(44) Pimenta, M. A.; Dresselhaus, G.; Dresselhaus, M. S.; Cançado, L. G.; Jorio, A.; Saito, R. Studying Disorder in Graphite-Based Systems by Raman Spectroscopy. *Phys. Chem. Chem. Phys.* **2007**, *9*, 1276−1290.
(45) Küper, S.; Brannon, J.; Brannon, K. Threshold Behavior in Polyimide Photoablation: Single-Shot Rate Measurements and Surface-Temperature Modeling. *Appl. Phys. A* **1993**, *56*, 43−50.
(46) Sharma, M.; Rani, S.; Pathak, D. K.; Bhatia, R.; Kumar, R.; Sameera, I. Temperature Dependent Raman Modes of Reduced Graphene Oxide: Effect of Anharmonicity, Crystallite Size and Defects. *Carbon* **2021**, *184*, 437−444.
(47) Wu, J.-B.; Lin, M. L.; Cong, X.; Liu, H. N.; Tan, P. H. Raman Spectroscopy of Graphene-Based Materials and Its Applications in Related Devices. *Chem. Soc. Rev.* **2018**, *47*, 1822−1873.
(48) Lan, Y.; Zondode, M.; Deng, H.; Yan, J. A.; Ndaw, M.; Lisfi, A.; Wang, C.; Pan, Y. le. Basic Concepts and Recent Advances of Crystallographic Orientation Determination of Graphene by Raman Spectroscopy. *Crystals* **2018**, *8*, No. 375.
(49) Mahmood, F.; Zhang, C.; Xie, Y.; Stalla, D.; Lin, J.; Wan, C. Transforming Lignin into Porous Graphene via Direct Laser Writing for Solid-State Supercapacitors. *RSC Adv.* **2019**, *9*, 22713−22720.
(50) Mamleyev, E. R.; Heissler, S.; Nefedov, A.; Weidler, P. G.; Nordin, N.; Kudryashov, Vv.; Länge, K.; MacKinnon, N.; Sharma, S. Laser-Induced Hierarchical Carbon Patterns on Polyimide Substrates for Flexible Urea Sensors. *npj Flexible Electron.* **2019**, *3*, No. 2.
(51) Cai, J.; Lv, C.; Watanabe, A. Laser Direct Writing of High-Performance Flexible All-Solid-State Carbon Micro-Supercapacitors for an on-Chip Self-Powered Photodetection System. *Nano Energy* **2016**, *30*, 790−800.
(52) Cai, J.; Lv, C.; Hu, C.; Luo, J.; Liu, S.; Song, J.; Shi, Y.; Chen, C.; Zhang, Z.; Ogawa, S.; Aoyagi, E.; Watanabe, A. Laser Direct Writing of Heteroatom-Doped Porous Carbon for High-Performance Micro-Supercapacitors. *Energy Storage Mater.* **2020**, *25*, 404−415.
(53) Jiang, Z.; Luo, J.; Yao, J.; Xu, C.; Liu, A.; Yao, Y.; Liu, T. Direct Laser Writing Carbonization Based on Internal-Reflection Setup for Fabricating Shape-Tailorable and Sealed in-Situ Carbon Features. *Mater. Des.* **2021**, *211*, No. 110162.
(54) Li, Y.; Xuan Luong, D.; Zhang, J.; Tarkunde, Y. R.; Kittrell, C.; Sargunaraj, F.; Ji, Y.; Arnusch, C. J.; Tour, J. M. Laser-Induced Graphene in Controlled Atmospheres: From Superhydrophilic to Superhydrophobic Surfaces. *Adv. Mater.* **2017**, *29*, No. 1700496.
(55) Imbrogno, A.; Islam, J.; Santillo, C.; Castaldo, R.; Sygellou, L.; Larrigy, C.; Murray, R.; Vaughan, E.; Hoque, Md. K.; Quinn, A. J.; Iacopino, D. Laser-Induced Graphene Supercapacitors by Direct Laser Writing of Cork Natural Substrates. *ACS Appl. Electron. Mater.* **2022**, *4*, 1541−1551.
(56) Mahmood, F.; Zhang, H.; Lin, J.; Wan, C. Laser-Induced Graphene Derived from Kraft Lignin for Flexible Supercapacitors. *ACS Omega* **2020**, *5*, 14611−14618.
(57) Chyan, Y.; Ye, R.; Li, Y.; Singh, S. P.; Arnusch, C. J.; Tour, J. M. Laser-Induced Graphene by Multiple Lasing: Toward Electronics on Cloth, Paper, and Food. *ACS Nano* **2018**, *12*, 2176−2183.
(58) Parmeggiani, M.; Zaccagnini, P.; Stassi, S.; Fontana, M.; Bianco, S.; Nicosia, C.; Pirri, C. F.; Lamberti, A. PDMS/Polyimide Composite as an Elastomeric Substrate for Multifunctional Laser-Induced Graphene Electrodes. *ACS Appl. Mater. Interfaces* **2019**, *11*, 33221−33230.
(59) Xia, S.-Y.; Long, Y.; Huang, Z.; Zi, Y.; Tao, L.-Q.; Li, C.-H.; Sun, H.; Li, J. Laser-Induced Graphene (LIG)-Based Pressure Sensor and Triboelectric Nanogenerator towards High-Performance Self-Powered Measurement-Control Combined System. *Nano Energy* **2022**, *96*, No. 107099.
(60) Jeong, S. Y.; Lee, J. U.; Hong, S. M.; Lee, C. W.; Hwang, S. H.; Cho, S. C.; Shin, B. S. Highly Skin-Conformal Laser-Induced Graphene-Based Human Motion Monitoring Sensor. *Nanomaterials* **2021**, *11*, No. 951.
(61) Reina, M.; Scalia, A.; Auxilia, G.; Fontana, M.; Bella, F.; Ferrero, S.; Lamberti, A. Boosting Electric Double Layer Capacitance in Laser-Induced Graphene-Based Supercapacitors. *Adv. Sustainable Syst.* **2022**, *6*, No. 2100228.
(62) Hyeong, S.-K.; Park, M.; Kim, S.-I.; Park, S.; Choi, K.-H.; Im, M. J.; Kim, N. D.; Kim, T.-W.; Lee, S. H.; Park, J.-W.; Bae, S.; Lee, J.-H.; Lee, S.-K. Compacted Laser-Induced Graphene with Bamboo-Like Carbon Nanotubes for Transformable Capacitive Energy Storage Electrodes. *Adv. Mater. Technol.* **2021**, No. 2101105.
(63) Ren, M.; Zhang, J.; Tour, J. M. Laser-Induced Graphene Hybrid Catalysts for Rechargeable Zn-Air Batteries. *ACS Appl. Energy Mater.* **2019**, *2*, 1460−1468.
(64) You, R.; Liu, Y. Q.; Hao, Y. L.; Han, D. D.; Zhang, Y. L.; You, Z. Laser Fabrication of Graphene-Based Flexible Electronics. *Adv. Mater.* **2020**, *32*, No. 1901981.
(65) Gaur, A. P. S.; Xiang, W.; Nepal, A.; Wright, J. P.; Chen, P.; Nagaraja, T.; Sigdel, S.; Lacroix, B.; Sorensen, C. M.; Das, S. R. Graphene Aerosol Gel Ink for Printing Micro-Supercapacitors. *ACS Appl. Energy Mater.* **2021**, *4*, 7632−7641.
(66) Chen, H.; Chen, S.; Zhang, Y.; Ren, H.; Hu, X.; Bai, Y. Sand-Milling Fabrication of Screen-Printable Graphene Composite Inks for High-Performance Planar Micro-Supercapacitors. *ACS Appl. Mater. Interfaces* **2020**, *12*, 56319−56329.
(67) Li, F.; Qu, J.; Li, Y.; Wang, J.; Zhu, M.; Liu, L.; Ge, J.; Duan, S.; Li, T.; Bandari, V. K.; Huang, M.; Zhu, F.; Schmidt, O. G. Stamping Fabrication of Flexible Planar Micro-Supercapacitors Using Porous Graphene Inks. *Adv. Sci.* **2020**, *7*, No. 2001561.
(68) Esfahani, M. Z.; Khosravi, M. Stamp-Assisted Flexible Graphene-Based Micro-Supercapacitors. *J. Power Sources* **2020**, *462*, No. 228166.
(69) Karbhal, I.; Basu, A.; Patrike, A.; Shelke, Mv. Laser Patterning of Boron Carbon Nitride Electrodes for Flexible Micro-Supercapacitor with Remarkable Electrochemical Stability/Capacity. *Carbon* **2021**, *171*, 750−757.
(70) Liu, B.; Zhang, Q.; Zhang, L.; Xu, C.; Pan, Z.; Zhou, Q.; Zhou, W.; Wang, J.; Gu, L.; Liu, H. Electrochemically Exfoliated Chlorine-Doped Graphene for Flexible All-Solid-State Micro-Supercapacitors with High Volumetric Energy Density. *Adv. Mater.* **2022**, *34*, No. 2106309.
(71) El-Kady, M. F.; Kaner, R. B. Scalable Fabrication of High-Power Graphene Micro-Supercapacitors for Flexible and on-Chip Energy Storage. *Nat. Commun* **2013**, *4*, No. 1475.

(72) Shi, X.; Zhou, F.; Peng, J.; Wu, R.; Wu, Z. S.; Bao, X. One-Step Scalable Fabrication of Graphene-Integrated Micro-Supercapacitors with Remarkable Flexibility and Exceptional Performance Uniformity. *Adv. Funct. Mater.* **2019**, *29*, No. 1902860.
(73) Zang, X.; Shen, C.; Chu, Y.; Li, B.; Wei, M.; Zhong, J.; Sanghadasa, M.; Lin, L. Laser-Induced Molybdenum Carbide−Graphene Composites for 3D Foldable Paper Electronics. *Adv. Mater.* **2018**, *30*, No. 1800062.
(74) Lu, K.; Ma, Y.; Ye, J. Combination of Chemical Foaming Strategy and Laser-Induced Graphene Technology for Enhanced Paper-Based Microsupercapacitor. *J. Power Sources* **2022**, *535*, No. 231488.
(75) Wang, M.; Chen, J.; Lu, K.; Ma, Y.; Li, H.; Ye, J. Preparation of High-Performance Flexible Microsupercapacitors Based on Papermaking and Laser-Induced Graphene Techniques. *Electrochim. Acta* **2022**, *401*, No. 139490.
(76) Tang, H.; Chen, R.; Huang, Q.; Ge, W.; Zhang, X.; Yang, Y.; Wang, X. Scalable Manufacturing of Leaf-like MXene/Ag NWs/Cellulose Composite Paper Electrode for All-Solid-State Supercapacitor. *EcoMat* **2022**, No. e12247.
(77) Huang, Q.; Yang, Y.; Chen, R.; Wang, X. High Performance Fully Paper-Based All-Solid-State Supercapacitor Fabricated by a Papermaking Process with Silver Nanoparticles and Reduced Graphene Oxide-Modified Pulp Fibers. *EcoMat* **2021**, *3*, No. e12076.
(78) Rao, Y.; Yuan, M.; Luo, F.; Wang, Z.; Li, H.; Yu, J.; Chen, X. One-Step Laser Fabrication of Phosphorus-Doped Porous Graphene Electrodes for High-Performance Flexible Microsupercapacitor. *Carbon* **2021**, *180*, 56−66.
(79) Yuan, M.; Luo, F.; Wang, Z.; Li, H.; Rao, Y.; Yu, J.; Wang, Y.; Xie, D.; Chen, X.; Wong, C. P. Facile and Scalable Fabrication of High-Performance Microsupercapacitors Based on Laser-Scribed in Situ Heteroatom-Doped Porous Graphene. *ACS Appl. Mater. Interfaces* **2021**, *13*, 22426−22437.
(80) Li, N.; Jiang, K.; Rodríguez-Hernández, F.; Mao, H.; Han, S.; Fu, X.; Zhang, J.; Yang, C.; Ke, C.; Zhuang, X. Polyarylether-Based 2D Covalent-Organic Frameworks with In-Plane D−A Structures and Tunable Energy Levels for Energy Storage. *Adv. Sci.* **2022**, *9*, No. 2104898.

https://doi.org/10.1021/acsami.2c09667
ACS Appl. Mater. Interfaces 2022, 14, 46427−46438